

Micro- and Nanomotors as Active Environmental Microcleaners and Sensors

Jemish Parmar, Diana Vilela*, Katherine Villa, Joseph Wang*, and Samuel Sánchez*

Accepted version at Journal of the American Chemical Society - June 2018

Corresponding Authors

Diana Vilela - Institute for Bioengineering of Catalonia (IBEC), The Barcelona Institute of Science and Technology, Baldiri Reixac 10-12, 08028 Barcelona Spain; Orcid: <http://orcid.org/0000-0001-5005-7070> ; Email: dvilela@ibecbarcelona.eu

Joseph Wang - Department of NanoEngineering, University of California San Diego, La Jolla, California 92093, United States; Orcid: <http://orcid.org/0000-0002-4921-9674> ; Email: josephwang@ucsd.edu

Samuel Sánchez - Institute for Bioengineering of Catalonia (IBEC), The Barcelona Institute of Science and Technology, Baldiri Reixac 10-12, 08028 Barcelona Spain; Institució Catalana de Recerca i Estudis Avancats (ICREA), Pg. Lluís Companys 23, 08010 Barcelona, Spain; Orcid: <http://orcid.org/0000-0002-5845-8941> ; Email: ssanchez@ibecbarcelona.eu

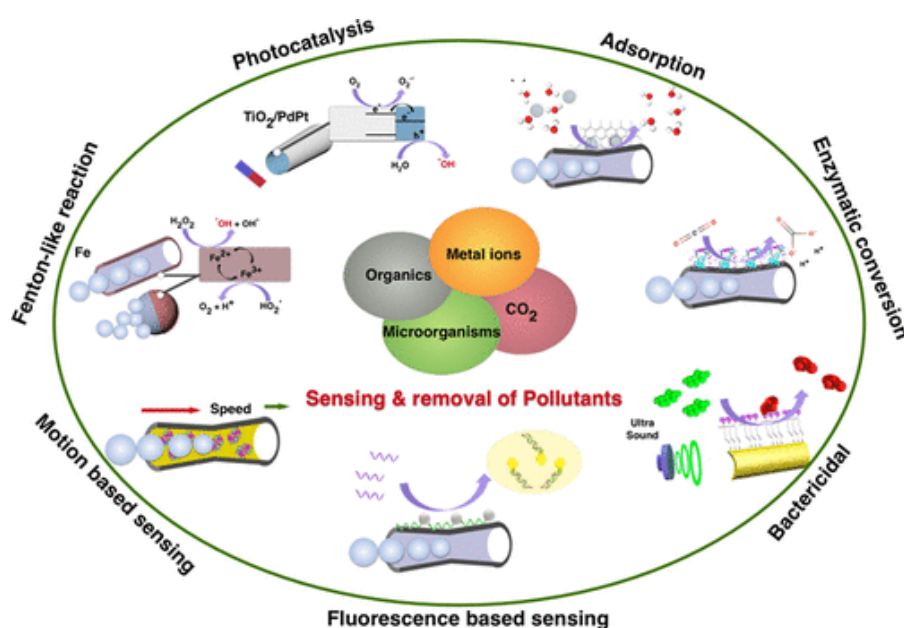
Authors

Jemish Parmar - Institute for Bioengineering of Catalonia (IBEC), The Barcelona Institute of Science and Technology, Baldiri Reixac 10-12, 08028 Barcelona Spain; Orcid: <http://orcid.org/0000-0001-7561-7417>

Katherine Villa - Institute for Bioengineering of Catalonia (IBEC), The Barcelona Institute of Science and Technology, Baldiri Reixac 10-12, 08028 Barcelona Spain; Orcid: <http://orcid.org/0000-0003-1917-0299>

Abstract

The quest to provide clean water to the entire population has led to a tremendous boost in the development of environmental nanotechnology. Toward this end, micro/nanomotors are emerging as attractive tools to improve the removal of various pollutants. The micro/nanomotors either are designed with functional materials in their structure or are modified to target pollutants. The active motion of these motors improves the mixing and mass transfer, greatly enhancing the rate of various remediation processes. Their motion can also be used as an indicator of the presence of a pollutant for sensing purposes. In this Perspective, we discuss different chemical aspects of micromotors mediated environmental cleanup and sensing strategies along with their scalability, reuse, and cost associated challenges.



Introduction

Water pollution is a major societal issue of the current century. Despite the progress in water treatment technologies, (1,2) people still lack access to clean drinking water. (3) Hence, there is a considerable need for developing faster and more advanced water treatments and new technologies to provide clean water for human beings and to prevent damage to the environment, aquatic life, and other living organisms.

Microorganisms can swim at a low Reynolds number by moving their cellular appendages. (4) When these microorganisms swim together, they can create turbulent flows that are often strong enough to promote the mixing in water bodies. Inspired by nature, various types of artificial micro/nanomotors have been developed in the past decade, which can propel at low Reynolds number. (5) Micro/nanomotors have been the subject of a tremendous interest in recent years owing to their great potential to perform a broad range of complex tasks in different fields. (6–8) The movement of micro/nanomotors has been shown to impart efficient micromixing and enhance mass transfer which would otherwise be limited to passive diffusion. (9,10) The enhancement of mass transfer in chemical reactions is relatively easy to achieve for the macro- and mesoscale using blending or turbulent dispersions. (11) However, efficient micromixing at the molecular scale is extremely challenging. This difficulty arises from the fact

that at the low Reynolds numbers, flows are inherently laminar so the micromixing is dominated by passive diffusion. (12)

Micro/nanomachines act as artificial active matter which can enhance the reaction yields and reduce the treatment times by overcoming the diffusion-limited reactions and improving the interactions between their active surface and target pollutants. In the case of bubble-propulsion mechanism, bubbles can create additional mixing along with the three-dimensional swimming of the micromotors. (13) Leveraging these attractive properties, researchers have recently developed a wide range of applications, ranging from removal of pollutants from water to direct sensing of pollutants.

In this Perspective, we will focus on the chemical aspects and the specific chemical functionalization of the surface of micro/nanomotors and the way they can be adapted for versatile chemical applications in water remediation. We review key strategies and distinct designs of micro/nanomotors as mobile cleaning platforms that greatly enhance and accelerate the removal of inorganic, organic, and biological pollutants. Also, we discuss their pollutant removal mechanisms and challenges (e.g., scalability and reusability) related to their use toward practical environmental applications.

Fabrication of Micro/Nanomotors

Micro/nanomotors designed for environmental applications contain functional materials that enable their swimming at the microscale and removal of pollutants from the contaminated water. The choice of the functional material depends on the target pollutants. Apart from the chemistry of the functional material, the mode of propulsion of micromotors also depends on their design and shape. Usually, the micromotors used for the environmental application have tubular or spherical shape and are commonly bubble-propelled. Tubular micromotors are mainly fabricated by either roll-up nanotechnology or template-assisted synthesis. In the roll-up method (Figure 1A), strain engineered nanomembranes with the gradient of tensile strain in the first layer and compressive strain in the following layer are deposited on photoresist patterns. The etching of these patterns induce a strain release process of the nanomembranes that leads to rolling of the nanomembranes into tubular structures. (14) In the case of porous template-assisted synthesis (Figure 1B), polycarbonate (PC) membranes with conically shaped micropores are used as templates. (15) The walls of the pores are initially coated with electrodeposited polymers, metal, or graphene layers that act as the outer motor layer, followed by deposition of the inner catalytic layer and release of the resulting open tubes by dissolving the PC templates. Instead of electrodeposition, chemical methods such as sol-gel synthesis and metal ion reduction are also used for tubes fabrication. (16) The inner layer of tubular micromotors, obtained from both fabrication methods, contains a catalyst (Pt, MnO₂, Pd) which decomposes very quickly the chemical fuel, usually hydrogen peroxide (H₂O₂) into oxygen (O₂) bubbles. The bubbles are expelled from one end of the tubular structure and create propulsion forces that push the tubular structure on the opposite direction. (17–19) Anodized alumina templates are used to make rod-like nano/micromotors with bimetallic composition or magnetic materials by electrodeposition in the nanopores. These bimetallic micromotors are propelled by self-electrophoresis mechanism, in which one side of the micromotor has a catalytic metal that can decompose H₂O₂. The micromotor acts as a tiny battery where the electrons generated during the fuel decomposition travel through the conductive bimetallic structure while the protons travel on the surface of the micromotor and

drag along water molecules that create propulsion forces for the motion. (20) In the case of micromotors with a magnetic material, a controlled external magnetic field is used to propel them. Rod-like micromotors with certain geometrical features at the one end of the structure can also be propelled by ultrasound due to local the pressure gradients that ultrasounds generate. (21)

Figure 1

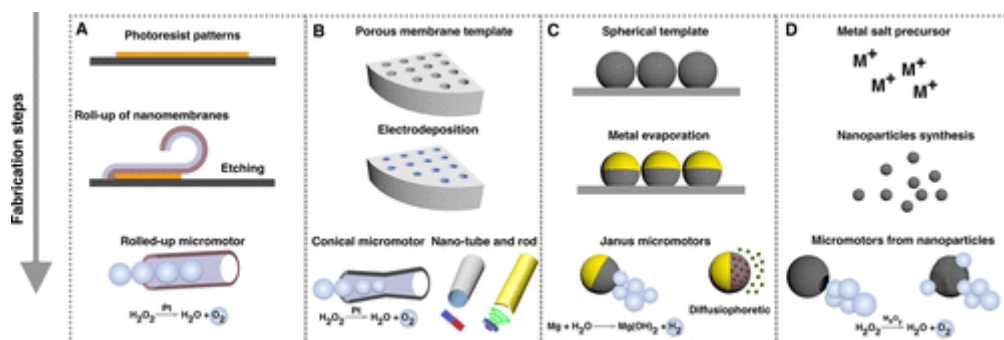


Figure 1. Fabrication of micromotors using (A) roll-up technique, (B) porous template-assisted synthesis, (C) spherical template and physical vapor deposition, and (D) assembly of nanoparticles.

Spherical micromotors are fabricated by using solid spheres in which a layer of a material is deposited by physical vapor deposition techniques to make Janus particles. The solid spheres and the deposited material can be catalytic or noncatalytic depending on the target application of the Janus micromotor (Figure 1C). Janus microparticles with a catalyst coating are usually propelled by so-called diffusiophoresis mechanism in which the diffusion of product molecules creates a fluid flow around the micromotors. (22) The noncatalytic micromotors used for environmental applications usually contain magnesium which reacts with water to produce hydrogen gas (H₂) for bubble propulsion. (23) More recently, micromotors were fabricated by the assembly of nanoparticles, synthesized from metal salt solutions as precursors (Figure 1D). This kind of micromotors are either made by emulsion-assisted soft templating in which geometries and sizes can be controlled as well as the asymmetry in the structure for an efficient propulsion (24) or by using aggregates of nanoparticles. (25) The nanoparticles present in the structure act as a catalyst to decompose H₂O₂ into O₂ bubbles for the propulsion.

The external surface of the micromotors is either made of functional materials or chemically modified to attach functional molecules that can degrade or remove pollutants from the contaminated water or perform sensing of contaminants. Such surface modification is selected based on the target pollutants present in the contaminated water and their chemistry. Functional micromotors can thus participate in a variety of environmental remediation processes.

Chemical Functionalization of Micromotors and Mechanisms for Removal of Pollutants

Heavy Metals

The presence of heavy metal ions in water bodies and drinking water can have severe health effects on the population and aquatic systems. Micromotors designed for heavy metals removal include adsorptive materials, chelating agents, or quantum dots in their structure. Carbon-based micro/nanomaterials have shown high adsorptive properties for several kinds of pollutants. Particularly, activated carbon is one of the most common and low-cost materials for the removal of heavy metals and other contaminants from water, owing to their high density of surface active sites, short intraparticle diffusion distance, tunable pore size, and a wide surface chemistry. The first report using Janus micromotors for the removal of heavy metals was published by Jurado-Sánchez et al. (26) They used one-sided granulated activated carbon spheres as adsorbent material for the removal of lead ions (Pb^{2+}) and platinum on their other side for their self-propulsion without further modification (Figure 2Aa). The self-propelled activated Janus spheres led to higher yields (~ 12 -fold in 1 min) for the removal of Pb^{2+} in comparison with the static activated particles. Another carbon allotrope, graphene, has demonstrated to be an efficient adsorbent for various heavy metal ions. Taking advantage of this property, Vilela et al. designed graphene oxide-based micromotors (GOx micromotors) for the removal of heavy metals from water. (27) These micromotors have tubular structure and are synthesized by template-based electrochemical deposition of graphene, nickel, and platinum (Figure 2Ab). The graphene oxide on the surface of GOx-micromotors acts as a Lewis base by its oxygen moieties and delocalized π -electron system, while Pb^{2+} and Hg^{2+} act as Lewis acids by their free atomic orbitals. Compared to nonmotile micromotors, the removal of Pb^{2+} was much higher for the self-propelled approach (Figure 2Ac). As a proof of concept of heavy metals recovery, authors used a microfluidic system to demonstrate that once the micromotors adsorb the metal pollutants, they can be magnetically driven from one location to another, and then, at the desired location, heavy metal ions can be released from the surface of micromotors in a strong acidic environment, allowing the reuse of the micromotors. Thus, such systems can be used to cleanup heavy metal pollution and concentrate them for their further recovery. In addition to carbon-based materials, thiol groups are also used to functionalize micromotors for heavy metals chelation. Self-propelled chelation platform described by Wang's group contains magnesium-based Janus spherical micromotors with a gold layer deposited on one side of the micromotors. (28) The meso-2,3-dimercaptosuccinic acid self-assembled onto the gold surface of the Janus micromotors introduced functional groups, such as thiol and carboxylic groups (Figure 2Ad). While one thiol group is attached to the gold surface, the remaining thiol and carboxylic moieties can capture Zn^{2+} , Cd^{2+} , and Pb^{2+} present in the aqueous media via chelation. These functionalized Mg/Au Janus micromotors effectively cleaned wastewater containing these three heavy metals (0.5 ppm, each) in < 4 min.

Figure 2

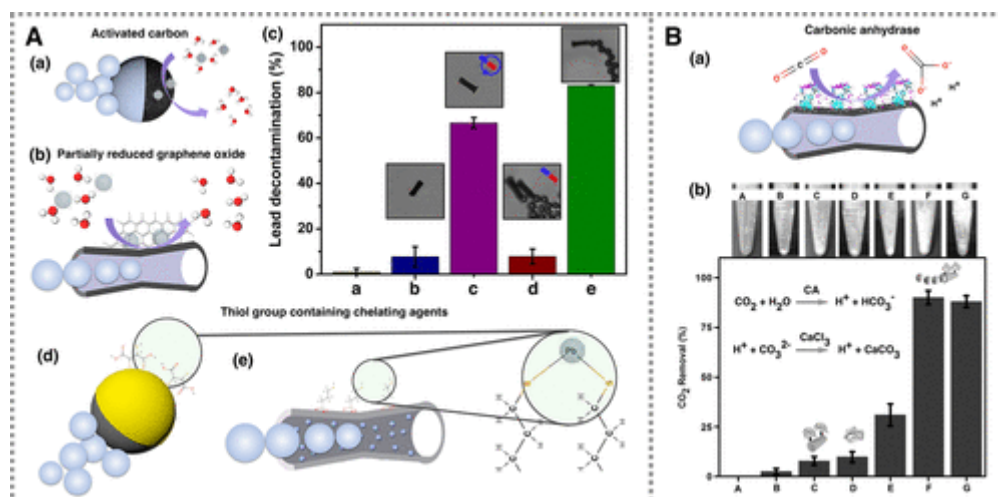


Figure 2. Removal of inorganic pollutants using micromotors. (A) Adsorptive removal of heavy metal pollutants on micromotors with the functionalized outer surfaces. The design of micromotors with (a) activated carbon and (b) graphene oxide as the functional surfaces and the plot (c) of the percentage decontamination by graphene oxide-based micromotors (80% removal) compared to the decontamination by static micromotors (20% removal) clearly show the importance of the self-propulsion (adapted from ref (27); copyright 2016 American Chemical Society. (d and e) Functionalization using a thiol-containing chelating agent on gold and silica surface. (B) Carbon dioxide sequestration using micromotors: (a) carbonic anhydrase enzyme functionalized micromotors and (b) enhanced removal of carbon dioxide mineralization into calcium carbonate by self-propelled micromotors compared to static micromotors and free enzyme present in the solution (adapted with permission from ref (33); copyright 2015 John Wiley & Sons, Inc.).

In a different approach, Escarpa et al. fabricated tubular micromotors decorated with nanocrystals on their surfaces for the removal of heavy metals and organic compounds using different mechanisms. (29) These micromotors were synthesized by co-electrodeposition of aniline with zinc and sulfur in a membrane-template to form ZnS nanocrystals, followed by Pt electrodeposition. Since the thiol group has a high affinity for heavy metals such as Hg²⁺, a cation-exchange process provoked its binding on the micromotors, forming HgS. The removal of Hg²⁺ was confirmed by the mercury EDX detection and the decrease of the fluorescence caused by the substitution of ZnS nanocrystals by HgS on the micromotor surface. Instead of using electrochemical systems and/or metal sputtering techniques, Vilela et al. developed a facile chemical route (membrane-based template combined with sol-gel synthesis) to fabricate tubular mesoporous silica-based micromotors which are able to clean Pb²⁺ contamination from water. (16) Inside the tubular structure, PtNPs were synthesized by chemical reduction of PtCl₂ salt to facilitate self-propulsion in the presence of H₂O₂. The outer silica surface was functionalized by attaching a silane molecule, (3-mercaptopropyl) trimethoxysilane via condensation (Figure 2Ae). The thiol group in the silane acted as a chelating agent to capture Pb²⁺ on the surface of the micromotors. In a similar design by the same group, PtNPs have been replaced by MnO₂ as the catalyst for propulsion, and the outer surface was decorated with photocatalytic γ -Fe₂O₃NPs to remove heavy metals (Cd²⁺ and Pb²⁺) and different organic molecules. (30) As an alternative approach, Pumera's group used DNA-functionalized catalytic micromotors (31) and natural sporopollenin exine capsules (SECs) (32) for the removal of mercury and lead ions, respectively. In their work, one side of the SECs

was coated with platinum to enable self-propulsion of the particle in H₂O₂, while the open surface acted as a natural adsorbent for the removal of Pb²⁺ from polluted water.

Carbon Dioxide

Carbon dioxide (CO₂) emissions and its further accumulation are directly related to the climate change and global warming. Uygun et al. reported an approach to capture CO₂ using micromotors modified with carbonic anhydrase (CA) on their surfaces for CO₂ sequestration in water and storage as solid carbonate salts. (33) These template electrodeposited (COOH-polymer/Pt) tubular micromotors have been modified with CA on the surface using carbodiimide cross-linker chemistry (Figure 2Ba). The CA-modified micromotors were able to convert CO₂ to bicarbonate ions (HCO₃⁻) while they swim in the presence of H₂O₂. To avoid the CA equilibrium between CO₂ and bicarbonate species, CaCl₂ was added to the solution for carrying out the precipitation of HCO₃⁻ in the form of calcium salt (CaCO₃) and activating the equilibrium of the conversion of CO₂ to HCO₃⁻. The motile CA functionalized micromotors were 5 times more efficient in removing CO₂ compared to static micromotors with the same functionalization (Figure 2Bb). Table 1 shows the list of micro/nanomotors reported for the removal of inorganic pollutants.

Table 1. Micro/Nanomotors for the Removal of Inorganic Pollutants^a

Inorganic pollutants	Motor design	Mechanism	Propulsion	fuel	Ref.
Pb ²⁺		Physisorption	$2\text{H}_2\text{O}_2 \xrightarrow{\text{Pt}} \text{O}_2 + 2\text{H}_2\text{O}$	H ₂ O ₂	26
Pb ²⁺ Hg ²⁺		Physisorption (Lewis acid-based)	$2\text{H}_2\text{O}_2 \xrightarrow{\text{Pt}} \text{O}_2 + 2\text{H}_2\text{O}$	H ₂ O ₂	27
Pb ²⁺ Zn ²⁺ Cd ²⁺		Physisorption (chelation)	$\text{Mg} + 2\text{H}_2\text{O} \rightarrow \text{H}_2 + \text{Mg}^{2+} + 2\text{OH}^-$	Mg/H ₂ O	28
Hg ²⁺		Physisorption (ion-exchange)	$2\text{H}_2\text{O}_2 \xrightarrow{\text{Pt}} \text{O}_2 + 2\text{H}_2\text{O}$	H ₂ O ₂	29
Pb ²⁺		Physisorption (chelation)	$2\text{H}_2\text{O}_2 \xrightarrow{\text{Pt}} \text{O}_2 + 2\text{H}_2\text{O}$	H ₂ O ₂	16
Pb ²⁺ Cd ²⁺		Physisorption	$2\text{H}_2\text{O}_2 \xrightarrow{\text{MnO}_2} \text{O}_2 + 2\text{H}_2\text{O}$	H ₂ O ₂	30
Pb ²⁺		Physisorption	$2\text{H}_2\text{O}_2 \xrightarrow{\text{Pt}} \text{O}_2 + 2\text{H}_2\text{O}$	H ₂ O ₂	32
CO ₂		Conversion and precipitation	$2\text{H}_2\text{O}_2 \xrightarrow{\text{Pt}} \text{O}_2 + 2\text{H}_2\text{O}$	H ₂ O ₂	33

^aSome parts in the table are adapted with permissions from the respective copyright holders.

Oil Removal

Oil pollution is a major environmental concern, especially during large oil spills, that can damage to a large extent the aquatic life. Self-propelled platforms can be an interesting and useful tool to capture and transport oil pollutants because of their motion capabilities. The

first example of micromotors removing oil pollutants was reported by Guix et al. in 2012. (34) They synthesized PEDOT/Pt tubular micromotors by electrodeposition method in PC template, and then, one side of their long axis was coated with a gold film. These micromotors, powered by catalytic decomposition of H₂O₂ by their inner Pt layer, were functionalized on their external gold surface with superhydrophobic n-alkanethiols chains with different lengths which formed self-assembly monolayers (SAM). The presence of long carbon chains renders the surface of micromotors hydrophobic, which can attract oil droplets molecules via hydrophobic interactions. Authors noted that longer chains (C12) were more efficient for capturing oil droplets than smaller chains (C6). However, by increasing the chain length to C18, the inner platinum surface was blocked thus hindering the movement of the micromotors. Also, it was observed that the speed of the micromotors with the oil droplet on their surface decreased up to 10 times from the original speed. These results established that it is possible to capture pollutants “on the fly” mechanism via superhydrophobic surface modifications of micromotors. In a follow-up work, the same group used Mg/Au Janus micromotors for oil removal. (35) In this work, the gold hemisphere cap of these magnesium based Janus micromotors was functionalized with dodecanethiol molecules. The authors demonstrated that these micromotors, as the earlier reported work, removed oil droplets being powered even by seawater. However, one disadvantage is their shortened lifespan (10–15 min) due to the self-consumption of magnesium during the motion. In a different design, Mou et al. synthesized micromotors without any noble metals using oleic acid modified MnFe₂O₄ nanoparticles. (24) Taking advantage of the hydrophobic nature of oleic acid, the oleic acid modified nanoparticles were self-assembled into hollow microspheres with a single hole via emulsion templating method. The hollow microspheres move because of the catalytic decomposition of H₂O₂ into oxygen bubbles and water by MnFe₂O₄ NPs in their interior. In addition, the oleic acid molecules embedded in the structure make the internal and external surfaces superhydrophobic for capturing 1-octane oil droplets (Figure 3A). One of the major advantages of this approach is that the micromotors can be prepared in large quantities without using noble metals and expensive methods. However, these motors still required the use of H₂O₂ for their propulsion. Zhao et al. fabricated a magnetic-controlled millimeter-sized polymer capsule motor with various functionalities, which moves by the Marangoni effect. This effect is produced due to the changes of the surface tension provoked by the release of an organic solvent from the motor. These motors swam in a wide variety of liquid/air interfaces (water, seawater, organic solvent/water mixtures, and acids), and they were capable of merging several oil droplets and cleaning the water surfaces. (36)

Figure 3

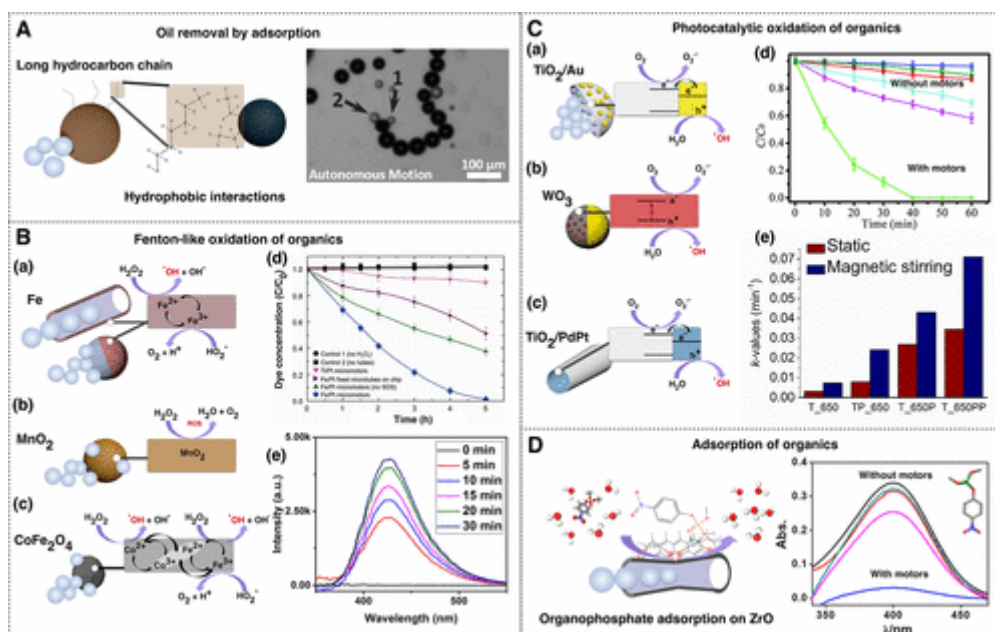


Figure 3. Removal of oil and organic pollutants using micromotors. (A) Removal and transport of oil by micromotors functionalized with long hydrocarbon chains (adapted with permission from ref (24); copyright 2015 John Wiley & Sons, Inc.). (B) Chemistry of production of reactive oxidative species by Fe (a), MnO₂ (b), and CoFe₂O₄ (c) containing micromotors for oxidation of organic pollutants in the presence of hydrogen peroxide. (d) Fast removal of organic dye by iron-containing self-propelled micromotors (adapted from ref (9); copyright 2013 American Chemical Society). (e) Detection of hydroxyl radicals produced by cobalt ferrite micromotors during removal of pharmaceutical pollutant (adapted with permission from ref (25); copyright 2017 Elsevier). (C) Chemistry of photocatalytic micromotors with TiO₂/Au (a), WO₃ (b), and TiO₂/PdPt (c) propelled by bubbles, self-diffusiophoresis, and external magnetic field, respectively. (d and e) Accelerated photocatalytic removal of pollutants by self-propelled and externally propelled micromotors, respectively (adapted with permission from refs (41 and 42); copyright 2016 Royal Society of Chemistry and copyright 2016 John Wiley & Sons, Inc., respectively). (D) Adsorption of organophosphate warfare agents on the zirconia-functionalized micromotors surfaces. Inset shows the enhanced removal of the organophosphate by swimming micromotors (adapted from ref (43); copyright 2015 American Chemical Society).

Organic Molecules

Industrial and anthropogenic activities generate a large amount of organic waste, such as pesticides, pharmaceuticals, insecticides, dyes, among others. Most of these pollutants are highly toxic (even in low concentrations) and often cannot be decomposed by current biological treatments. Interestingly, most organic molecules can be degraded using advanced oxidation processes (AOPs). These AOPs play an important role in the complete removal of these recalcitrant organic pollutants through the generation of highly oxidizing species such as hydroxyl (HO•), superoxide (O₂•⁻), and hydroperoxyl (HO₂•) radicals. Among them, Fenton and photocatalysis are the most promising methods because of their moderate cost and high efficiency. The Fenton reaction, which characterizes by the reaction of an iron salt with H₂O₂ under acidic pH, generates HO• and HO₂• radicals which are able to degrade organic molecules with high efficiency. Photocatalysis, on the other hand, consists on the activation of a semiconductor material to carry out oxidation–reduction reactions for the degradation of

organic pollutants under light irradiation. The excitation of a photocatalyst, such as TiO_2 , with proper wavelength ($h\nu \geq E_g$), generates electron–hole pairs. Then, the holes react with the water or hydroxyl groups adsorbed on the surface to generate hydroxyl radicals, meanwhile, the photogenerated electrons react with the oxygen in the media to produce superoxide radicals and H_2O_2 . Given the high oxidizing potential of these species, they carry out the total mineralization of organic molecules to CO_2 , water, and some nonharmful inorganic salts.

Micromotors designed to carry out Fenton-like or photocatalytic oxidation reactions contain active Fenton or photocatalytic materials in their structure. These micromotors result in efficient decontamination processes due to the micromixing which enhances these surface reactions while swimming in the contaminated media. Moreover, they can be easily recovered from the solution by the incorporation of a magnetic layer in their structure (usually Ni and Fe), facilitating the whole decontamination process. (37) In 2013, Soler et al. synthesized Fe/Pt micromotors by rolled-up technique to degrade rhodamine 6G (R6G), as a model pollutant of xanthene dyes via Fenton-like reaction (Figure 3Ba). (9) The iron (Fe) on the external surface acted as Fenton catalyst for the generation of $\text{HO}\cdot$ radicals against R6G and provided magnetic properties to the micromotors. The total degradation of R6G was achieved after 5 h of swimming of micromotors, while the static Fe/Pt tubes only achieved around 50% degradation (Figure 3Bd). In addition, it was observed that the efficiency of the R6G degradation was dependent on the thickness of the Fe layer on the micromotors, pH, and concentration of H_2O_2 . To prove the cost-effectiveness of these Fe/Pt micromotors, Parmar et al. demonstrated that these micromotors can continuously swim for a long period of time (>24 h) and be reused during several decontamination cycles of malachite green (MG), a common dye that causes carcinogenic symptoms. Furthermore, they degraded more than 80% of MG in <1 h and also observed that after the first cycle of degradation, micromotors were mainly acting as a heterogeneous Fenton-like catalyst. (38) However, the mass production of this type of tubular micromotor is still limited to expensive techniques such as rolled-up procedures. Teo et al. presented zerovalent nanomotors (Fe^0) that can be prepared in ton quantities by thermally induced solid-state reduction of an Fe precursor for the degradation of dyes. (39) Two toxic dyes, methylene blue (MB) and methyl orange (MO), were degraded after only 15 min of treatment with Fe^0 nanomotors in an acidic environment. These nanomotors self-propelled by the production of H_2 bubbles from the reaction of citric acid with Fe. Recently, Li et al. developed a facile and scalable method for fabrication of $\text{AgNPs}/\text{SiO}_2@/\text{Fe}_3\text{O}_4$ Janus micromotors based on polydopamine chemistry for the degradation of MB. (40) In this configuration, Fe_3O_4 acts as a Fenton-like catalyst, which is self-propelled by the decomposition of H_2O_2 on the Ag. These micromotors showed almost a total degradation of MB compared to 59% degradation using $\text{Fe}_3\text{O}_4/\text{SiO}_2$ microparticles at the same reaction time (8 h). These results confirm the important role of the bubbled-propelled mechanism on the enhancement of organic pollutants removal.

Besides iron, other transition-metal oxides such as MnO_2 can also carry out Fenton-like reactions under a similar mechanism for degradation of dyes (Figure 3Bb). Thus, taking advantage of its ability for decomposing H_2O_2 , this low-cost material has been used as catalyst for propulsion of micromotors and simultaneously to remove textile waste such as R6G and MB, by Fenton-like mechanism. Additionally, the separation of organic dyes through adsorption on the surface of gas bubbles generated by MnO_2 micromotors (in the presence of surfactants) also contributes to dye removal. (44,45) The scalable synthesized tubular $\text{SiO}_2/\text{MnO}_2$ micromotors decorated with $\gamma\text{-Fe}_2\text{O}_3$ NPs reported by Villa et al. resulted in a fast degradation of RB and tetracycline (TC), and efficient removal of heavy metal ions (Cd^{2+} and

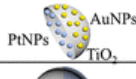
Pb²⁺). (30) In this kind of approach, the authors combined the photocatalytic activity and adsorptive properties of Fe₂O₃ along with the Fenton-like activity of MnO₂ in a single micromotor. This work shows the potential of metal-oxide-based micromotors for the simultaneous removal of different kind of pollutants (dyes, pharmaceutical and heavy metal waste) present in wastewater and synthesis of tubular micromotors without using electrochemical synthesis methods. In a different scalable synthesis approach, Parmar et al. fabricated micromotors from aggregated cobalt ferrite nanoparticles, which cannot propel individually by bubble propulsion but self-propel when aggregated into few micrometer-sized particles. (25) The authors reported removal of tetracycline antibiotic without the need of adding surfactants in the system. They proposed that the cobalt ferrite micromotors can enhance production of hydroxyl radicals via Fenton-like reaction due to the presence of cobalt (Figure 3Bc). In this study, fluorescence-based hydroxyl radical detection technique was used to confirm the production of these highly oxidative radical by the cobalt ferrite micromotors (Figure 3Be).

Considering that dyes and other organic molecules can be degraded through photocatalytic reactions, photocatalytic micromotors were fabricated for the removal of dyes in the presence of light. (41,42,46–48) One of the most efficient photocatalysts, TiO₂, has been employed for the fabrication of photocatalytic micromotors because of its large band gap, low cost, and abundance. For instance, TiO₂-based micromotors propelled by the catalytic decomposition of H₂O₂ by PtNPs have been reported for the removal of dyes such as MB, MO, and rhodamine B (RB) in wastewater. (41) They were synthesized using template-assisted aqueous phase method by modifying a 5 μm polystyrene (PS) microparticle with PtNPs and then sputtering one side with TiO₂, modifying the surface with AuNPs and final PS calcination at high temperatures H₂O₂ (Figure 3Ca). These micromotors showed high efficiencies for MB degradation compared to different conditions without micromotors due to the plasmonic-photocatalytic mechanism in the presence of solar light along with the strong mass transfer produced by the O₂ bubbles generated from H₂O₂ (Figure 3Cd). Likewise, fuel-free Pt-TiO₂ and Au-WO₃@C Janus micromotors, synthesized by ion sputtering of Pt or Au on one-half, respectively, can be propelled and controlled by UV-light radiation for the degradation of two dyes, dichlorophenolindophenol (DCIP) and RB. (46,47) The Janus morphology of both micromotors leads to the asymmetrical generation of electrons and ions on each part of the structure, resulting in a self-electrophoretic (Pt-TiO₂) or self-difusiophoretic (Au-WO₃@C) motion mechanism (Figure 3Cb). A step forward toward real applications involves the development of photocatalytic systems active under visible light (a major component of solar radiation).

TiO₂ is photoactive solely under UV light, which is 5% of the solar light, due to its wide band gap. Thus, to obtain response into visible light, TiO₂ can be doped or coupled with metals, semiconductors, and nonmetals. Pané and co-workers have developed coaxial TiO₂/noble metal (Pd, PtPd) nanotubes (NTs) filled with nickel nanowires (NWs) for the photocatalytic remediation of dyes (MB, MO, and RB) under visible and natural light. (42) These TiO₂/(Pd, PtPd)NTs have been synthesized using a sequential template-assisted electrodeposition of TiO₂, Pd, or PtPd and Ni. The hybrid nanomotors (TiO₂/PtPdNTs) demonstrated higher photocatalytic activity than TiO₂/PdNTs because of the coupling of noble metals to TiO₂ generating electron–hole pairs under visible light (Figure 3Cc). These TiO₂-PtPd coaxial NTs degraded 100% of RB in 30 min under natural sunlight, after that, they were recovered from the solution using a magnet for their further reuse. The magnetic actuation of these micromotors was shown to improve the photocatalytic degradation rate of the pollutant while

compared with the static micromotors (Figure 3Ce). The same group designed Bi₂O₃/BiOCl-based hybrid microbots activated by UV–vis irradiation and controlled by an external magnetic field for the efficient removal of RB. (48) These hybrid micromotors were synthesized using a similar method in two different shapes, micropillars and microhelices, consisting of a ferromagnetic segment followed by a bismuth-based photocatalytic segment. They exhibited 90% efficiency for the removal of RB, being a good example of biocompatible, low-cost, and wirelessly powered micromotors for water cleaning treatments. Tubular CdS-PANI-Pt micromotors with photocatalytic activity have been reported for removal of Bisphenol A (BPA), a widely distributed environmental pollutant, which exhibits toxic, endocrine, mutagenic, and carcinogenic effects in living organisms. (29) These CdS-based micromotors, synthesized by the membrane-template method, as described above, degraded BPA under solar light irradiation obtaining removal efficiencies between 85 and 100% depending on the initial level of the BPA contamination. Other pollutants such as phenolic compounds have also been efficiently degraded by different micromotor-based approaches. For instance, p-nitrophenol (p-NP), which is a common waste of textile, pharmaceutical, and agriculture industries, was totally removed by rolled-up Cr/Fe/Ti/Pd microjets. (37) These micromotors were self-propelled by the H₂ production from the reaction between Pd and NaBH₄ on their inner surface. Pd particles were integrated into the micromotor structure by drop casting on top of the metal thin films (Cr/Fe/Ti), using an e-beam evaporator on squares made of a sacrificial material. The Pd thin films were then rolled up into the micromotor structure. Pd-based micromotors degraded over 95% of p-NP in <5 min of the reaction period. Table 2 shows the list of micro/nanomotors reported for the removal of organic pollutants.

Table 2. Micro/Nanomotors for the Removal of Organic Pollutants^a

Organic pollutants	Motor design	Mechanism	Propulsion	fuel	Ref.
Oil		Physisorption (hydrophobic interaction)	$2\text{H}_2\text{O}_2 \xrightarrow{\text{Pt}} \text{O}_2 + 2\text{H}_2\text{O}$	H_2O_2	34
Motor oil		Physisorption (hydrophobic interaction)	$\text{Mg} + 2\text{H}_2\text{O} \rightarrow \text{H}_2 + \text{Mg}^{2+} + 2\text{OH}^-$	$\text{Mg}/\text{H}_2\text{O}$	35
1-Octane oils		Physisorption (hydrophobic interaction)	$2\text{H}_2\text{O}_2 \xrightarrow{\text{Pt}} \text{O}_2 + 2\text{H}_2\text{O}$	H_2O_2	24
Oil		Physisorption (hydrophobic interaction)	Marangoni effect	.	36
Rhodamine 6G Malachite green		Degradation (Fenton oxidation)	$2\text{H}_2\text{O}_2 \xrightarrow{\text{Pt}} \text{O}_2 + 2\text{H}_2\text{O}$	H_2O_2	9,38
Methylene blue Methyl Orange		Degradation (Fenton oxidation)	$2\text{Fe} + 6\text{C}_6\text{H}_5\text{O}_7 \rightarrow 9\text{H}_2 + 2\text{Fe}(\text{C}_6\text{H}_5\text{O}_7)_3$	$\text{C}_6\text{H}_5\text{O}_7$	39
Methylene blue		Degradation (Fenton like oxidation)	$2\text{Ag} + 2\text{H}_2\text{O}_2 \rightarrow 2\text{Ag}^+ + \text{O}_2 + 2\text{H}_2\text{O}$	H_2O_2	40
Methylene blue Rhodamine 6G		Degradation (Fenton like oxidation) Adsorptive bubble separation	$2\text{H}_2\text{O}_2 \xrightarrow[\text{H}^+]{\text{MnO}_2} \text{O}_2 + 2\text{H}_2\text{O}$	H_2O_2	44,45
Tetracycline Rhodamine B		Degradation (Fenton like oxidation)	$2\text{H}_2\text{O}_2 \xrightarrow{\text{MnO}_2} \text{O}_2 + 2\text{H}_2\text{O}$	H_2O_2	30
Tetracycline		Degradation (Fenton like reaction)	$2\text{H}_2\text{O}_2 \xrightarrow{\text{CoFe}_2\text{O}_4} \text{O}_2 + 2\text{H}_2\text{O}$	H_2O_2	25
Methylene blue Methyl Orange Rhodamine B		Degradation (Plasmonic photocatalysis)	$2\text{H}_2\text{O}_2 \xrightarrow{\text{Pt}} \text{O}_2 + 2\text{H}_2\text{O}$	H_2O_2	41
Rhodamine B		Degradation (Photocatalysis)	Photoinduced self-electrophoretic	UV light	46
Rhodamine B DCIP		Degradation (Photocatalysis)	Photo induced diffusiophoresis	UV light	47
Methylene blue Methyl Orange Rhodamine B		Degradation (Photocatalysis)	Magnetic field	light	42
Rhodamine B		Degradation (Photocatalysis)	Magnetic field	UV-Vis	48
Bisphenol A		Degradation (Photocatalytic)	$2\text{H}_2\text{O}_2 \xrightarrow{\text{Pt}} \text{O}_2 + 2\text{H}_2\text{O}$	H_2O_2	29
p-Nitrophenol		Degradation (Catalytic reduction)	$\text{NaBH}_4 + 4\text{H}_2\text{O} \xrightarrow{\text{Pd}} 4\text{H}_2 + \text{NaB}(\text{OH})_4$	NaBH_4	37
Methyl-paraoxon Ethyl-paraoxon		Degradation (Photocatalytic)	$\text{Mg} + 2\text{H}_2\text{O} \rightarrow \text{H}_2 + \text{Mg}^{2+} + 2\text{OH}^-$	H_2O	23
2,4-dinitrotoluene Methyl-paraoxon Rhodamine 6G		Physisorption	$2\text{H}_2\text{O}_2 \xrightarrow{\text{Pt}} \text{O}_2 + 2\text{H}_2\text{O}$	H_2O_2	26
PBDES Triclosan (POPs)		Physisorption	$2\text{H}_2\text{O}_2 \xrightarrow{\text{Pt}} \text{O}_2 + 2\text{H}_2\text{O}$	H_2O_2	49
Methyl-paraoxon Ethyl-paraoxon Bis-4-nitrophenylphosphate		Physisorption (Lewis acid-based)	$2\text{H}_2\text{O}_2 \xrightarrow{\text{Pt}} \text{O}_2 + 2\text{H}_2\text{O}$	H_2O_2	43
diethyl chlorophosphate (DCP)		Physisorption (Lewis acid-based)	$2\text{H}_2\text{O}_2 \xrightarrow{\text{Ag}} \text{O}_2 + 2\text{H}_2\text{O}$	H_2O_2	50
2-Amino-4-Chlorophenol *also Azo-dyes		Degradation (enzymatic oxidation)	Marangoni Effect	.	51
2-Amino-4-Chlorophenol Catechol Guaiacol		Degradation (enzymatic oxidation)	$2\text{H}_2\text{O}_2 \xrightarrow{\text{Catalase}} \text{O}_2 + 2\text{H}_2\text{O}$	H_2O_2	53

^aSome parts in the table are adapted with permissions from the respective copyright holders.

Micromotors have also been designed for the removal of chemical warfare agents (CWA) and persistent organic pollutants (POPs), mainly by adsorption and/or photocatalytic reactions on their surface. Li et al. synthesized TiO₂/Mg microspheres for the degradation of CWAs by depositing TiO₂ on magnesium spheres. (23) In the presence of UV light, TiO₂/Mg micromotors can oxidize methyl-paraoxon (MP) and ethyl-paraoxon (EP), highly toxic organophosphate nerve agents, by the generation of reactive oxygen species on their surface. Janus activated carbon/Pt microspheres reported by Jurado-Sánchez et al. can also remove MP, apart from the removal of lead ions and other organic molecules, by its adsorption on the activated carbon. (26) Graphene can also be used for adsorption of organic pollutants because of π -interactions with some organic compounds. Orozco et al. reported a similar design of spherical micromotors, but instead of activated carbon microsphere, they used silica microspheres coated with reduced graphene oxide (rGO) layers. (49) Half of the microsphere was later coated with a Pt layer for its self-propulsion in the presence of H₂O₂. They reported that SiO₂@rGO-Pt Janus micromotors were able to remove polybrominated diphenyl ethers (PBDEs) and triclosan as persistent organic pollutants (POPs) models from the contaminated water. In addition, authors demonstrated the reuse of these micromotors after four cycles of reaction. Singh et al. reported zirconia (ZrO) graphene tubular micromotors to remove multiple extremely toxic organophosphate compounds (Figure 3D). (43) These micromotors were electrochemically synthesized using graphene as the outer layer and platinum as the inner layer. Since π -interactions between organophosphates and graphene were not strong enough to remove these pollutants from the contaminated solution, ZrO was immobilized on the graphene surface by electrochemical reduction of zirconium chloride. Results (Figure 3D, plot) showed a significant role of ZrO for the effective removal of MP, EP, and bis-4 nitrophenyl phosphate (b-NPP) via acid–base Lewis interaction of negatively charged oxygen atoms present in OP with the electronically deficient zirconia. These composite graphene-based micromotors showed 91, 70, and 58% removal of MP, EP, and NPP, respectively. Sarin, another organophosphorus ester compound, is a potent toxic for the nervous system. To remove this lethal compound, multifunctional silver-exchanged zeolite micromotors have been designed to catalytically degrade diethyl chlorophosphate (DCP), a sarin simulant. (50) The Ag-zeolite motors were synthesized by ion exchange between commercial 45 μ m zeolite and silver nitrate, and then one side was coated with Ag layer using sputtering process. The silver ion into the aluminosilicate zeolite framework favored a strong binding to DCP, followed by their “on the fly” effective hydrolysis, reaching 90% DCP degradation. In the future, with sufficient development, this kind of “on the fly” adsorption and degradation system could be an alternative to conventionally activated carbon filters to remove in situ various kind of pollutants.

Alternatively, biocatalytic reactions can also be used for selective degradation of pollutants. Orozco et al. demonstrated that self-propelled tubular motors degraded chemical pollutants by releasing an enzyme. (51) The motors consist of millimeter plastic tips filled with a mix of laccase enzyme, surfactant (SDS), and water and closed with wax in the wide edge. Once the lacasse-based motors were placed in contaminated water with 2-amino-chlorophenol (2-A-4CP), they released the enzyme along with the SDS producing an efficient biocatalytic degradation of phenols from the solution. The high concentration of SDS solution inside the tubes provoked Marangoni forces resulting in an efficient circular locomotion of these motors. This efficient movement enhanced the enzyme–substrate interactions, and compared to the diffusion of free enzyme, the degradation efficacy was greatly improved. Using the same propulsion mechanism and taking advantage of the mixing properties of motors, Zhao et al.

developed polysulfone (PSf) particles loaded with SDS with the ability to sweep the flucculated pollutant while they swim inside of a maze. (52) Another approach using biocatalytic reactions for the degradation of pollutants removed guaiacol, catechol, and 2-A-4CP in the presence of radish tissue biomotors propelled by the enzymatic decomposition of H₂O₂, mediated by the catalase/peroxidase on their surface. (53) It was observed that the decontamination efficiency of these plant-based motors was correlated with the variations in the level of both enzymes. Furthermore, the milliscale of these enzymatic-based motors could be beneficial to reach large areas of pollution and speed up the decontamination process without external mixing force.

Pathogenic Microorganisms

The presence of pathogens in the water is a leading cause for the increase in diseases such as cholera and typhoid. Common disinfection methods use chemicals (chlorine, chloramines, and ozone) or physical processes (UV light and heat) or a combination of both due to the high resistance of some pathogens. However, the high doses of these disinfectants can be harmful or may leave toxic byproducts. Micromotors focused on the removal of pathogenic bacteria from contaminated water, integrating on their structures several bactericidal materials or molecules such as enzymes, polymers, and metals have been developed. Additionally, these micromotors can be designed for the selective isolation and destruction of bacteria by the modification of their structure with aptamers, antibodies, protein receptors, and target enzymes. Campuzano et al. described the first example of micromotors for capturing and isolating bacteria. First, Ni/Au layers were deposited by e-beam vapor deposition on the outer surface of electrosynthesized polyaniline (PANI)/Pt tubular micromotors. (54) Afterward, the Au surface was modified using mercaptoundecanoic acid and NHS/EDC chemistry for the subsequent incorporation of the lectin receptor. Once the lectin-modified micromotors were placed in H₂O₂ solution, they selectively bind to the Escherichia coli (E. coli) surface by antibody–antigen interactions and capture E. coli while swimming. Later, the same research group demonstrated the first use of nanomotors for killing bacteria. The team used porous gold nanowires (p-AuNWs) propelled with an external ultrasound (US) source and functionalized their surface with lysozyme, an antibacterial peptidoglycan-hydrolase (muramidase activity) enzyme (Figure 4A) able to damage specifically the protective wall of bacteria. (55) The p-AuNWs were fabricated using template electrosynthesis of different metal layers: (i) Ag sacrificial layer, (ii) Au layer, and (iii) Au–Ag layer being liberated after silver removal. The surface was chemically modified with cysteamine, which forms Au–S bonds and provides N-terminal groups to the AuNWs, for the subsequent use of glutaraldehyde molecule as a linker of proteins. Two kinds of bacteria, *Micrococcus lysodeikticus* and E. coli, were rapidly destroyed by these named “nanofighters” in comparison with static lysozyme–AuNWs and free lysozyme. This fact was attributed to the enhancement of lysozyme–bacteria interactions because of the fluid mixing generated by the nanomotors motion. After this pioneering approach, several studies have described different micromotors decorated with other antibacterial molecules, such as chitosan or silver-based materials. Spherical water propelled micromotors made of chitosan/alginate poly(lactide-co-glycolide)/alginate/gold/magnesium (Chi/Alg/PLGA/Au/Mg) have been reported for E. coli decontamination (Figure 4B). (56) Chitosan is a hydrophilic polycationic biopolymer industrially obtained by N-deacetylation of chitin and is able to interact with negatively charged cell membranes, such as bacteria walls, leading to the leakage of proteinaceous and other intracellular constituents. These chitosan-based micromotors showed a high bactericidal effect

while they were swimming in comparison with the static analogous and the nonchitosan-based micromotors. As in the previous study, the autonomous propulsion of the Chi/Alg/PLGA/Au/Mg micromotors in drinking-water provided fluid mixing and, consequently, improved the chitosan-micromotor contact with bacteria interactions and its bactericidal efficiency.

Figure 4

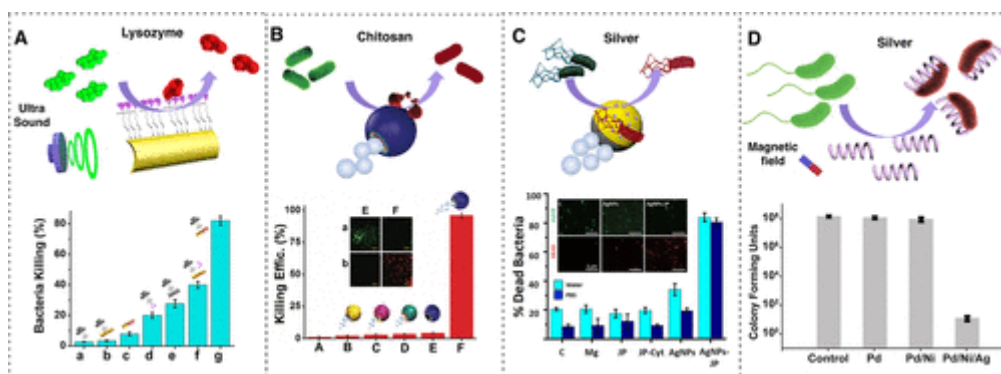


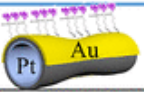
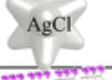
Figure 4. Removal of pathogenic microorganisms by (A) ultrasound propelled nanomotors containing lysozyme (adapted from ref (55); copyright 2015 American Chemical Society), (B and C) chitosan and silver nanoparticle-coated bubble propelled magnesium-based micromotors (adapted with permission from refs (56 and 57); copyright 2017 Royal Society of Chemistry and copyright 2017 American Chemical Society, respectively), and (D) magnetically propelled silver layer coated helical micromotors. Plots in each part illustrate the improved neutralization of the microorganism by respective swimming micromotors (adapted with permission from ref (58); copyright 2016 John Wiley & Sons, Inc.).

Silver, in the metal (Ag₀) and ion form (Ag⁺), has been widely used as a bactericidal material for the treatment of injuries, wounds, and infections. Ag⁺ and Ag₀ bind to the proteins present on the bacteria walls, disrupting their functionality and its permeability, leading to the cell lysis and death. Taking advantage of the silver bactericidal properties, several Ag-based micro/nanomotors approaches have been developed for bacteria decontamination purposes. Silver-coated nanocoils, which are magnetically driven by external magnetic fields, are demonstrated to efficiently kill bacteria (Figure 4D). (58) The helical structures of the nanocoils are made of three metals: Pd as template material and Ni and Ag, which provide magnetic and bactericidal properties, respectively. They were fabricated by template-assisted co-electrodeposition of Pd and Cu in AAO template, followed by deposition of Ni and Ag nanolayers using physical vapor deposition. The resulting nanocoils, capable of swimming in water by low magnetic fields, displayed high bactericidal effect for two types of bacteria: *E. coli* and *Staphylococcus aureus*. Despite the hypothesis about the mechanism of the bactericidal action of Ag structures based on the release of Ag ions on the bacteria walls, here it was proved that, by using *E. coli* resistant to Ag⁺, the direct contact of the nanocoils with the bacteria started the membrane disintegration due to (i) the tendency of Ag to react with functional groups found on the bacterial walls (phosphorus-containing lipopolysaccharides or teichoic acids) which produced conformational changes and (ii) the generation of mechanical stress on the bacterial walls caused by the nanosized and roughness of the nanomotors.

Other groups have developed other silver-based approaches such as Janus microparticles based on Mg microparticles half covered with Ag (59) or decorated with AgNPs. (57) This approach resulted in more than 90% of *E. coli* death after 10 min of micromotors locomotion, however, the concentration of micromotors used was very high. The bactericidal effect was attributed to the Ag⁺ release from the bimetallic micromotors while they swim. (59) Vilela et al. have developed water self-propelled Janus micromotors decorated with AgNPs that are able to kill and remove bacteria from contaminated water (Figure 4C). (57) The synthesis of these micromotors was carried out by e-beam vapor deposition of iron and gold on a monolayer of Mg microparticles, followed by chemical functionalization of the gold surface with cysteamine. Negatively charged AgNPs were linked to the surface by electrostatic interaction with the positively charged amino groups of cysteamine. The antibacterial efficiency of these AgNP-coated micromotors was attributed to (i) the active motion of the micromotors which increases the diffusion and release of Ag⁺ ions and the chances of contact between the surface of bacteria with AgNPs and (ii) the reported tendency of bacteria to attach on precious metal surfaces that favors the bactericidal effect and speeds up the selective Ag⁺ released from these micromotors. (60) Furthermore, the magnetic Fe layer makes possible the magnetic control and the easy removal of these micromotors with the attached bacteria on their surfaces. Other geometries such as microstar-shaped micromotors have been fabricated using AgCl for the inhibition of bacteria growth and other environmental applications. (61) This work was inspired by using the light source to achieve motion of the photoactive AgCl particles. Besides demonstrating the inhibition of the bacteria growth, the AgCl microstars were also able to degrade a different kind of dye (model organic pollutants).

Bacillus anthracis is Gram-positive bacteria which exerts anthrax, a lethal toxin. This kind of pollutant is extremely toxic and has been commonly used as biological and chemical weapons. The anthrax spore (anti-*Bacillus globigii*) antibody modified (PPy)-COOH/PEDOT/Ni/Pt micromotor was developed for the selective capture and destruction of anthrax spores. (62) The antibody-modified micromotors were capable of targeting and capturing anthrax simulant spores while they moved in the presence of an excess of nontarget *S. aureus* and *E. coli* in PBS as well as in water. Furthermore, in a parallel assay, anthrax spores were exposed to unmodified micromotors. The fast movement of these motors provoked accelerated mixing and damage of the spore cell walls. Apart from that, photocatalytic TiO₂/Au/Mg micromotors self-propelled in water were designed to remove *B. globigii* spores. As previously described, the photogenerated hydroxyl and superoxide radicals and the in situ formation of H₂O₂ on the surface of the TiO₂-based micromotors lead to the destruction of the bacteria membrane and mineralization of the chemical pollutants. (23) Table 3 shows the list of micro/nanomotors reported for the removal of pathogenic microorganism.

Table 3. Micro/Nanomotors for the Removal of Pathogenic Microorganism^a

Pathogenic microorganism	Motor design	Mechanism	Propulsion	fuel	Ref.
<i>E. coli</i>		Selective capture (lectin)	$2\text{H}_2\text{O}_2 \xrightarrow{\text{Pt}} \text{O}_2 + 2\text{H}_2\text{O}$	H_2O_2	54
<i>M. Lysodeikticus</i> <i>E. Coli</i>		Enzymatic wall disruption (Muramidase activity)	Ultrasound	-	55
<i>E. coli</i>		Walls disruption (leakage of proteinaceous)	$\text{Mg} + 2\text{H}_2\text{O} \rightarrow \text{H}_2 + \text{Mg}^{2+} + 2\text{OH}^-$	$\text{Mg}/\text{H}_2\text{O}$	56
<i>E. Coli</i> <i>Staphylococcus Aureus</i>		Cell lysis (enzyme disruption from bacteria)	Magnetic fields	-	58
<i>E. Coli</i>		Cell lysis (enzyme disruption from bacteria)	$\text{Mg} + 2\text{H}_2\text{O} \rightarrow \text{H}_2 + \text{Mg}^{2+} + 2\text{OH}^-$	$\text{Mg}/\text{H}_2\text{O}$	59
<i>E. Coli</i>		Cell lysis (enzyme disruption from bacteria)	$\text{Mg} + 2\text{H}_2\text{O} \rightarrow \text{H}_2 + \text{Mg}^{2+} + 2\text{OH}^-$	$\text{Mg}/\text{H}_2\text{O}$	57
<i>E. Coli</i>		Cell lysis (enzyme disruption from bacteria)	Photoinduced self-electrophoretic	UV light	61
<i>Bacillus Globiggi</i> spores (Anthrax simulant)		Selective capture	$2\text{H}_2\text{O}_2 \xrightarrow{\text{Pt}} \text{O}_2 + 2\text{H}_2\text{O}$	H_2O_2	62
<i>Bacillus Globiggi</i> spores (Anthrax simulant)		Cell lysis (fast contact)	$2\text{H}_2\text{O}_2 \xrightarrow{\text{Pt}} \text{O}_2 + 2\text{H}_2\text{O}$	H_2O_2	62
<i>Bacillus Globiggi</i> spores (Anthrax simulant)		Degradation (Photocatalysis)	$\text{Mg} + 2\text{H}_2\text{O} \rightarrow \text{H}_2 + \text{Mg}^{2+} + 2\text{OH}^-$	$\text{Mg}/\text{H}_2\text{O}$	23

^aSome parts in the table are adapted with permissions of the respective copyright holders.

Micro/Nanomotors for Sensing of Pollutants

In the past decade, analytical chemistry has widely employed new micro- and nanodevices for sensing target (bio-) molecules. Micro/nanomotors have emerged as an alternative tool in this area, due to their special properties such as functional versatility, capacity of transporting, and isolating target molecules in complex media and enhancement of micromixing, which results in short-time analysis and enhanced sensitivity of (bio-) assays. Micromotors can also lead to new analytical concepts utilizing speed or distance as analytical signals. Three different (bio-) sensing approaches have been mainly reported in the bibliography: (i) motion-based sensing based on changes in the speed and movement of micro/nanomotors induced by the target analyte, (63–66) (ii) fluorescence “on–off” strategy, (67–73) and (iii) chemical reaction occurring on the surface of micro/nanomotors to improve external detection. (74)

Heavy Metal Ions

Inorganic pollutants, mostly metals, have been determined using motion-based sensing as a transduction mechanism. The first work that used that strategy was developed by Wang et al. in 2009. (63) This work resulted from the observation of changes in the swimming behavior of catalytic micro/nanomotor in the presence of different analytes. These changes in speeds and

trajectories of micro/nanomotors were correlated with the concentration of the target analyte at a fixed fuel concentration. Particularly, the authors observed a considerable increase of the speeds (5-fold) of catalytic bisegment Au–Pt nanowires in the presence of Ag⁺ in a solution containing 5% of H₂O₂ as fuel (Figure 5A). The acceleration of the Au–Pt nanowires because of Ag⁺ presence is explained by the superficial reduction of Ag⁺ on the nanomotors in the presence of H₂O₂ (underpotential deposition). The silver deposition onto a catalytic surface may change its catalytic properties, making both segments more catalytically active. On the contrary, the presence of other metals, such as heavy metals, has been detected by the decrease of the micromotor speeds. In a different approach, researchers have used synthetic self-propelled enzyme-based micro/nanomotors (75) which can be inhibited by several analytes. (64,76) For instance, catalase, an enzyme which breaks down H₂O₂ into oxygen and water, has been commonly used for the self-propulsion of artificial tubular micro/nanomotors. These catalase-based micromotors led to an efficient swimming behavior, reaching maximum speeds of 120 μm s⁻¹ at 2% of H₂O₂. However, common contaminants, such as Hg²⁺ and Cu²⁺, can inhibit the activity of catalase provoking highly sensitive changes in the swimming behavior of micromotors propelled by catalase, which can be optically visualized (Figure 5C). This inhibition is caused by the bonds with sulfhydryl (-SH) and amino moieties of the enzyme with Hg²⁺ and Cu²⁺, respectively, altering its shape and blocking its activity. Thus, the detection of pollutants that act as inhibitors of catalase was performed using catalase-based micromotors. (64) Pumera’s group developed electrochemically synthesized Cu/Pt micromotors for the sensing of Pb²⁺ and Cd²⁺. Similar to enzyme-propelled micromotors, heavy metal ions present in the solution can poison the platinum core of the micromotors, leading to a decrease in their speed. This decrease in the speed can be correlated to the concentration of the heavy metals in the solution up to certain concentration (77) (Figure 5B). In a sensing approach not directly related to the observation of motion, fluorescence technique has been used for “on-the-fly” optical detection of analytes based on the quenching of fluorescence molecules. The tubular PEDOT/Pt micromotors were prepared by electrodeposition and later modified with PSS (-) and poly(diallyldimethylammonium chloride (PDDA) (+) for the incorporation of fluorescence CdTe quantum dots (QDs) on their surface. (73) The motion of these self-propelled micromotors provoked the binding of low quantities of Hg²⁺ to the QDs which were quenched, leading to a decrease of the fluorescence emission. The reduction of the fluorescence emission showed linearity between 0 and 1 mg/L of Hg²⁺ in solution. In addition, the authors demonstrated the high selectivity of QDs-based micromotors to target free Hg²⁺ compared to other mercury species (CH₃Hg⁺) and coexisting ions (Pb²⁺ and Cu²⁺).

Figure 5

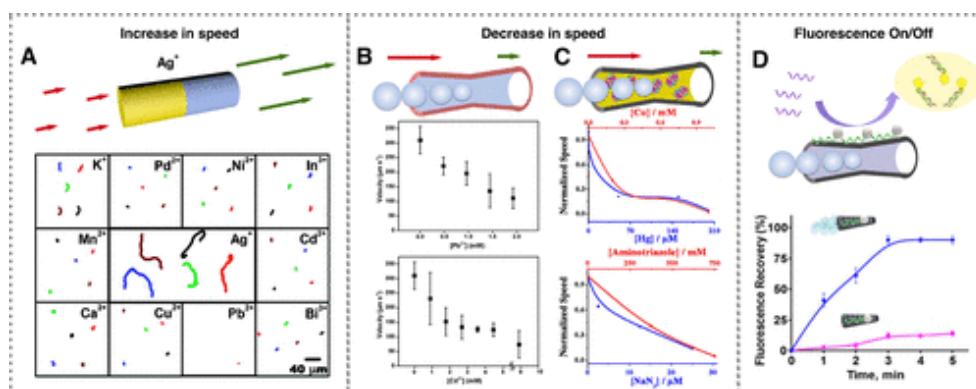


Figure 5. Sensing of pollutants using micromotors. (A) Detection of Ag⁺ by self-electrophoretic Au–Pt micromotors. The presence of the Ag⁺ increases the micromotor speed (adapted from ref (63); copyright 2009 American Chemical Society). (B and C) Detection of heavy metals (Pb, Cd, and Hg ions) and sodium nitrate by bubble propelled platinum and enzyme-based micromotors. The presence of these pollutants affects the propulsion of these micromotors and decreases their swimming speed. The plots represent the correlation of the micromotor speed with the pollutant concentration (adapted with permission from refs (64 and 66); copyright 2013 American Chemical Society and copyright 2014 John Wiley & Sons, Inc., respectively). (D) Micromotor-assisted fluorescence-based detection of pollutants. The motion of micromotors decreases the fluorescence recovery time for enhanced detection (adapted from ref (68); copyright 2016 American Chemical Society).

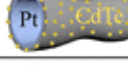
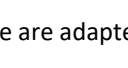
Organic Pollutants

Catalase-based micromotors were also used to detect nerve-agent vapor plumes, such as a sarin simulant (DCP), using motion-based sensing. (65) In this work, the presence of DCP vapor inhibited catalase activity, leading to a lower bubble-generation frequency and, consequently, the direct visualization of a weak locomotion of the micromotors.

As it has been previously introduced, micro/nanomotors can be functionalized on their surfaces by a wide variety of molecules. These molecules provide them with physical and chemical properties, such as fluorescence, capacity of recognition, and capturing. The “on–off” strategies are based on the fluorescence quenching methods for the effective and sensitive sensing of target analytes. The first fluorescent “on–off” micromotor strategy was reported in 2015 for the detection of sarin and soman simulants, as nerve agent models. (67) The Janus micromotors consisted of a silica microparticle with two faces with different functionalities, the sensing part covered with a dye (fluoresceinamine, FLA) and the catalytic counterpart with Pt. The self-propulsion of the dye-coated micromotors generated an effective fluid convection (without external force) due to the bubbles produced by the catalytic reaction on the Pt cap. In this work, the “on–off” is caused by the fast reaction of the phosphoryl halides, in the nerve agent simulant, with amino moieties of the FLA molecules. After this pioneer work, “on–off” strategies have been improved by the integration of selective molecules, such as aptamers, for the recognition of target analytes. Aptamers are single DNA strands that can be labeled with a fluorescent probe and are able to recognize and capture target molecules. Membrane-template electrodeposited graphene/Pt tubular micromotors have been used for “off–on” selective sensing of toxins (ricin) because they can attach on their surface aptamers by π -stacking interactions between carbon and nucleotide bases from the DNA (Figure 5D). (68) While the aptamer is confined on the micromotor surface, the dye did not show fluorescence. However, the fluorescence was restored upon binding of ricin to the aptamer receptor. To prove the high selectivity of these approaches, different proteins and toxins were used as interferents. Finally, the effect of the motion in the micromixing was demonstrated in comparison to static micromotors, displaying a dramatic enhancement of the fluorescent signal for the swimming micromotors which confirmed that the micromotor motion and the bubble trail induced a fluid convection favoring chemical reaction rates. Similar approaches based on the same “off–on” strategy using unmodified graphene/Pt (69) and graphene/Ni/Pt (70) micromotors along with fluorescent-labeled aptamers have been performed for the fast, simultaneous, and quantitative analysis of two mycotoxins (fumonisin B1, (FB1) and ochratoxin A, (OTA)) as contaminants in food samples.

Janus micromotors have been used for the simultaneous degradation and detection of persistent organic pollutants, such as phthalates (DPP), in food and biological samples. (74) In this work, simple Mg–Au Janus micromotors were placed on a screen-printed electrode. In presence of water, Mg–Au micromotors react with water producing H₂ bubbles and hydroxyl ions (OH⁻) which are able to swim and degrade phthalates in solution. The degradation of the phthalates produces phenol molecules which are electrochemically oxidized at lower potentials than phthalates. Thus, the localized OH⁻ ions generation and the autonomous Mg/Au micromotors movement resulted in an enhancement of the fluid mixing within a microliter sample droplet and an improved analytical performance for DPP detection in terms of sensitivity and selectivity (lowering the oxidation/detection potential). Table 4 shows the list of micro/nanomotors reported for the sensing of pollutants.

Table 4. Micro/Nanomotors for the Sensing of Pollutants^a

Analyte	Motor design	Mechanism	Propulsion	fuel	Ref.
Ag ⁺		Speed change (increasing of catalytic properties)	$H_2O_2 \xrightarrow{Pt} O_2 + 2H^+ + 2e^-$ $H_2O_2 + 2H^+ + 2e^- \xrightarrow{Au} 2H_2O$ Self-diffusiophoresis	H ₂ O ₂	63
Hg ²⁺ Cu ²⁺		Speed change (enzyme inhibition)	$2H_2O_2 \xrightarrow{Catalase} O_2 + 2H_2O$	H ₂ O ₂	64
Pb ²⁺ Cd ²⁺		Speed change (metal poisoning)	$2H_2O_2 \xrightarrow{Pt} O_2 + 2H_2O$	H ₂ O ₂	77
Hg ²⁺		Fluorescence "On-off" detection (Quenching of QDs)	$2H_2O_2 \xrightarrow{Pt} O_2 + 2H_2O$	H ₂ O ₂	73
Hg ²⁺		Fluorescence "On-off" detection (Quenching of QDs)	$2H_2O_2 \xrightarrow{Pt} O_2 + 2H_2O$	H ₂ O ₂	29
DCP (Sarin simulant)		Speed change (enzyme inhibition)	$2H_2O_2 \xrightarrow{Catalase} O_2 + 2H_2O$	H ₂ O ₂	65
DCP (Sarin simulant)		Fluorescence "On-off" detection	$2H_2O_2 \xrightarrow{Pt} O_2 + 2H_2O$	H ₂ O ₂	67
Ricin		Selective fluorescence "Off-on" detection	$2H_2O_2 \xrightarrow{Pt} O_2 + 2H_2O$	H ₂ O ₂	68
Fumonisin B1/Ochratoxin (Mycotoxins)		Selective fluorescence "Off-on" detection	$2H_2O_2 \xrightarrow{Pt} O_2 + 2H_2O$	H ₂ O ₂	69,70
Phthalates (DPP)		Favors Post-electrochemical analysis	$Mg + 2H_2O \rightarrow H_2 + Mg^{2+} + 2OH^-$	Mg/H ₂ O	74
Endotoxins from Pathogenic Bacteria		Selective fluorescence "Off-on" detection	$2H_2O_2 \xrightarrow{Pt} O_2 + 2H_2O$	H ₂ O ₂	71
<i>Salmonella enterica</i>		Selective fluorescence "Off-on" detection	$2H_2O_2 \xrightarrow{Pt} O_2 + 2H_2O$	H ₂ O ₂	72

^aSome parts in the table are adapted with permissions from the respective copyright holders.

Pathogenic Bacteria

Jurado-Sanchez et al. have used a Janus micromotor-based “on–off” detection strategy for bacterial endotoxins. (71) To synthesize these novel Janus micromotors, a 10% SDS water solution (containing graphene QDs modified with a fluorescent molecule) with chloroform (containing a polymer, PtNPs, and Fe₃O₄ NPs) was mixed under vigorous stirring. Afterward, the organic solvent evaporated to yield solidified polymer. The immiscibility of metal NPs with the polymer provoked their accumulation on one hemisphere of the synthesized microparticles producing the Janus asymmetry, which provides these micromotors an efficient propulsion and directionality in the presence of H₂O₂ and magnets, respectively. These Janus micromotors showed a mesoporous pore distribution, which allowed the diffusion of small molecules through the polymer. Thus, endotoxins released from the bacteria were able to diffuse to the interior of the micromotors, while they swam and cross-linked to the fluorescent molecule by quenching its fluorescence. As in the previous approaches, the active mixing component of micro/nanomotors played a crucial role in improving the speed and sensitivity of these bioassays. This approach was also used for the detection of *Salmonella enterica* by modifying the QDs with a receptor able to identify a component from the endotoxin structure. (72) The fluorescence quenching of the Janus micromotor by endotoxin from *Salmonella* and its dependence on the bacteria concentration allowed its quantification in food contaminated samples, such as egg yolk and egg white, mayonnaise, and milk.

Conclusions and Prospects

Since the first report on self-propelled nanomotors in 2004, there has been a tremendous progress in the field of micro/nanomotors. Particularly, these tiny machines have demonstrated to be effective tools for decontamination of several types of pollutants, including inorganic and organic molecules, generated mainly by anthropogenic and industrial activities. In comparison with passive particles, these micromotors exhibit dynamic motion and advanced functionalities, allowing higher remediation yields along with simpler and faster water cleaning processes than passive particles. Such improvement in water purification processes is due to the enhancement of the degradation and removal rates of the target pollutant. Owing to the magnetic control of micromotors during their motion, they are especially attractive for the potential removal of pollutants in remote areas, which cannot be easily accessed, and their further recovery after use. Additionally, the sensitivity of their motion behavior in relation to the environment, for example, presence of specific pollutants in wastewater, and/or their “on-the-fly” adsorption properties are appealing features for the development of miniaturized devices for the in situ detection of toxic chemicals and pathogenic microorganisms with fast response rates.

To expand the applicability of such micromotors to more realistic scenarios, some of the key limitations of current systems need to be addressed. One of the main challenges is related to the fabrication of micromotors via low-cost and scalable techniques. Currently common used fabrication methods require additional facilities, such as electrochemical stations, clean rooms, metal evaporators, or lithography platforms, which are expensive for the large-scale synthesis needed to clean up large volumes (m³) of contaminated water. Another economy related challenge is to avoid the use of expensive precious metals in the structure of micromotors. Different approaches dealing with their fabrication scalability and the use of alternative low-cost metals for their propulsion have been explored. For instance, there has been a transition

between micromotors that use mostly precious metals, such as Pt or Pd, to low-cost metal oxides, involving Mn-based oxides and Co and Fe ferrites. (24,25,39,44,48,78) Likewise, the preparation of micromotors based on merely synthetic chemical procedures has shown promise for their potential mass production. However, the structures synthesized by using these chemical methods are quite basic, usually containing a single material, and the methods do not allow much control for the synthesis of complex structures. Future efforts should be directed toward the development of scalable and low-cost synthesis methods for the fabrication of micromotors from inexpensive catalysts with multimaterials configurations.

Another important technical challenge that still requires attention is the use of the surfactants for the efficient propulsion of bubble-propelled micromotors. Surfactants ease the release of the bubble to facilitate their propulsion. Bubble-propelled micromotors are reported to swim either very slowly or not at all without surfactants. (79–81) Considering that these surfactants add extra organic load in the water and they can also compete with the pollutants during the degradation reaction, it may limit the overall efficiency of the performance of micromotors. Therefore, it is vital to ensure that micromotors do not leave any harmful reactants, byproducts, and other kinds of pollutants once their task is completed. Additionally, life-cycle assessments are required to evaluate the impact of the micromotors on the flora and fauna before and after the cleaning process.

Apart from that, the need of a chemical fuel can limit the application of micromotors for some environmental remediation purposes. Even though hydrogen peroxide, commonly used in many advanced oxidative processes, is considered a green reagent (that leaves only water and oxygen), micromotors designed for the adsorptive or antimicrobial activity should explore alternative propulsion strategies. Having on board active materials such as magnesium, zinc, or iron that react with water for propulsion and leave environmental friendly byproducts could be an attractive alternative if the fuel enables micromotors to function for long enough time to complete their task. Some of the remaining challenges to be addressed include special attention to the reusability of these micromotors for the removal of different kind of pollutants, including changes in the speed over usage time and maximum cycles of efficient decontamination. Moreover, the development of multifunctional micromotors that can simultaneously decontaminate different types of pollutants commonly found in wastewater, such as bacteria, heavy metals, or refractory organic pollutants, can pave way for highly efficient single-step universal water treatment technology.

Notes

The authors declare no competing financial interest.

Acknowledgments

The research leading to these results has received funding from the European Research Council ERC-2015-PoC/Project ID: 713608 (MICROCLEANERS). S.S. thanks the Spanish MINECO for grants CTQ2015-68879-R (MICRODIA) and CTQ2015-72471-EXP (Enzwim). D.V. acknowledges financial support provided by the European Commission under Horizon 2020s Marie Skłodowska-Curie Actions COFUND scheme [grant agreement no. 712754] and by the Severo Ochoa programme of the Spanish Ministry of Economy and Competitiveness [grant

SEV-2014-0425 (2015–2019)]. IBEC group thanks the CERCA Programme/Generalitat de Catalunya. J.W. acknowledges support from the Defense Threat Reduction Agency (grant HDTRA1-14-1-0064).

References

1. Shannon, M. A.; Bohn, P. W.; Elimelech, M.; Georgiadis, J. G.; Mariñas, B. J.; Mayes, A. M. *Nature* 2008, 452 (7185), 301, DOI: 10.1038/nature06599
2. Qu, X.; Brame, J.; Li, Q.; Alvarez, P. J. J. *Acc. Chem. Res.* 2013, 46 (3), 834– 843, DOI: 10.1021/ar300029v
3. Burek, P.; Satoh, Y.; Fischer, G.; Kahil, M. T.; Scherzer, A.; Tramberend, S.; Nava, L. F.; Wada, Y., et al., (2016) *Water Futures and Solution - Fast Track Initiative (Final Report)*. IIASA Working Paper. IIASA, Laxenburg, Austria: WP-16-006 Retrieved from <http://pure.iiasa.ac.at/id/eprint/13008/>
4. Purcell, E. M. *Am. J. Phys.* 1977, 45 (1), 3– 11, DOI: 10.1119/1.10903
5. Wang, H.; Pumera, M. *Chem. Rev.* 2015, 115 (16), 8704– 8735, DOI: 10.1021/acs.chemrev.5b00047
6. Wang, J. *Nanomachines: Fundamentals and Applications*; Wiley-VCH: Weinheim, 2013.
7. Sánchez, S.; Soler, L.; Katuri, J. *Angew. Chem., Int. Ed.* 2015, 54 (5), 1414– 1444, DOI: 10.1002/anie.201406096
8. Katuri, J.; Ma, X.; Stanton, M. M.; Sánchez, S. *Acc. Chem. Res.* 2017, 50 (1), 2– 11, DOI: 10.1021/acs.accounts.6b00386
9. Soler, L.; Magdanz, V.; Fomin, V. M.; Sanchez, S.; Schmidt, O. G. *ACS Nano* 2013, 7 (11), 9611– 9620, DOI: 10.1021/nn405075d
10. Orozco, J.; Jurado-Sánchez, B.; Wagner, G.; Gao, W.; Vazquez-Duhalt, R.; Sattayasamitsathit, S.; Galarnyk, M.; Cortés, A.; Saintillan, D.; Wang, J. *Langmuir* 2014, 30 (18), 5082– 5087, DOI: 10.1021/la500819r
11. Baldyga, J.; Bourne, J. R. *Chem. Eng. Sci.* 1992, 47 (8), 1839– 1848, DOI: 10.1016/0009-2509(92)80302-S
12. Knight, J. B.; Vishwanath, A.; Brody, J. P.; Austin, R. H. *Phys. Rev. Lett.* 1998, 80 (17), 3863– 3866, DOI: 10.1103/PhysRevLett.80.3863
13. Risso, F. *Annu. Rev. Fluid Mech.* 2018, 50 (1), 25– 48, DOI: 10.1146/annurev-fluid-122316-045003
14. Mei, Y.; Huang, G.; Solovev, A. A.; Ureña, E. B.; Mönch, I.; Ding, F.; Reindl, T.; Fu, R. K. Y.; Chu, P. K.; Schmidt, O. G. *Adv. Mater.* 2008, 20 (21), 4085– 4090, DOI: 10.1002/adma.200801589
15. Gao, W.; Sattayasamitsathit, S.; Orozco, J.; Wang, J. J. *Am. Chem. Soc.* 2011, 133 (31), 11862– 11864, DOI: 10.1021/ja203773g

16. Vilela, D.; Hortelao, A. C.; Balderas-Xicohténcatl, R.; Hirscher, M.; Hahn, K.; Ma, X.; Sánchez, S. *Nanoscale* 2017, 9 (37), 13990– 13997, DOI: 10.1039/C7NR04527A
17. Fomin, V. M.; Hippler, M.; Magdanz, V.; Soler, L.; Sanchez, S.; Schmidt, O. G. *IEEE Trans. Robot.* 2014, 30 (1), 40– 48, DOI: 10.1109/TRO.2013.2283929
18. Manjare, M.; Yang, B.; Zhao, Y.-P. *J. Phys. Chem. C* 2013, 117 (9), 4657– 4665, DOI: 10.1021/jp311977d
19. Parmar, J.; Vilela, D.; Sanchez, S. *Eur. Phys. J.: Spec. Top.* 2016, 225 (11–12), 2255– 2267, DOI: 10.1140/epjst/e2016-60064-x
20. Paxton, W. F.; Kistler, K. C.; Olmeda, C. C.; Sen, A., St.; St. Angelo, S. K.; Cao, Y.; Mallouk, T. E.; Lammert, P. E.; Crespi, V. H. *J. Am. Chem. Soc.* 2004, 126 (41), 13424– 13431, DOI: 10.1021/ja047697z
21. Esteban-Fernández de Ávila, B.; Martín, A.; Soto, F.; Lopez-Ramirez, M. A.; Campuzano, S.; Vásquez-Machado, G. M.; Gao, W.; Zhang, L.; Wang, J. *ACS Nano* 2015, 9 (7), 6756– 6764, DOI: 10.1021/acsnano.5b02807
22. Howse, J. R.; Jones, R. A. L.; Ryan, A. J.; Gough, T.; Vafabakhsh, R.; Golestanian, R. *Phys. Rev. Lett.* 2007, 99 (4), 048102, DOI: 10.1103/PhysRevLett.99.048102
23. Li, J.; Singh, V. V.; Sattayasamitsathit, S.; Orozco, J.; Kaufmann, K.; Dong, R.; Gao, W.; Jurado-Sanchez, B.; Fedorak, Y.; Wang, J. *ACS Nano* 2014, 8 (11), 11118– 11125, DOI: 10.1021/nn505029k
24. Mou, F.; Pan, D.; Chen, C.; Gao, Y.; Xu, L.; Guan, J. *Adv. Funct. Mater.* 2015, 25 (39), 6173– 6181, DOI: 10.1002/adfm.201502835
25. Parmar, J.; Villa, K.; Vilela, D.; Sánchez, S. *Appl. Mater. Today* 2017, 9, 605– 611, DOI: 10.1016/j.apmt.2017.11.002
26. Jurado-Sánchez, B.; Sattayasamitsathit, S.; Gao, W.; Santos, L.; Fedorak, Y.; Singh, V. V.; Orozco, J.; Galarnyk, M.; Wang, J. *Small* 2015, 11 (4), 499– 506, DOI: 10.1002/sml.201402215
27. Vilela, D.; Parmar, J.; Zeng, Y.; Zhao, Y.; Sánchez, S. *Nano Lett.* 2016, 16 (4), 2860– 2866, DOI: 10.1021/acs.nanolett.6b00768
28. Uygun, D. A.; Jurado-Sánchez, B.; Uygun, M.; Wang, J. *Environ. Sci.: Nano* 2016, 3 (3), 559– 566, DOI: 10.1039/C6EN00043F
29. Jurado-Sánchez, B.; Wang, J.; Escarpa, A. *ACS Appl. Mater. Interfaces* 2016, 8 (30), 19618– 19625, DOI: 10.1021/acsaami.6b05824
30. Villa, K.; Parmar, J.; Vilela, D.; Sánchez, S. *ACS Appl. Mater. Interfaces* 2018, 10 (24), 20478– 20486, DOI: 10.1021/acsaami.8b04353
31. Wang, H.; Khezri, B.; Pumera, M. *Chem.* 2016, 1 (3), 473– 481, DOI: 10.1016/j.chempr.2016.08.009
32. Wang, H.; Potroz, M. G.; Jackman, J. A.; Khezri, B.; Marić, T.; Cho, N.-J.; Pumera, M. *Adv. Funct. Mater.* 2017, 27 (32), 1702338, DOI: 10.1002/adfm.201702338
33. Uygun, M.; Singh, V. V.; Kaufmann, K.; Uygun, D. A.; de Oliveira, S. D. S.; Wang, J. *Angew. Chem., Int. Ed.* 2015, 54 (44), 12900– 12904, DOI: 10.1002/anie.201505155

34. Guix, M.; Orozco, J.; García, M.; Gao, W.; Sattayasamitsathit, S.; Merkoçi, A.; Escarpa, A.; Wang, J. *ACS Nano* 2012, 6 (5), 4445–4451, DOI: 10.1021/nn301175b
35. Gao, W.; Feng, X.; Pei, A.; Gu, Y.; Li, J.; Wang, J. *Nanoscale* 2013, 5 (11), 4696–4700, DOI: 10.1039/c3nr01458d
36. Zhao, G.; Seah, T. H.; Pumera, M. *Chem. - Eur. J.* 2011, 17 (43), 12020–12026, DOI: 10.1002/chem.201101450
37. Srivastava, S. K.; Guix, M.; Schmidt, O. G. *Nano Lett.* 2016, 16 (1), 817–821, DOI: 10.1021/acs.nanolett.5b05032
38. Parmar, J.; Vilela, D.; Pellicer, E.; Esqué-de los Ojos, D.; Sort, J.; Sánchez, S. *Adv. Funct. Mater.* 2016, 26 (23), 4152–4161, DOI: 10.1002/adfm.201600381
39. Teo, W. Z.; Zboril, R.; Medrik, I.; Pumera, M. *Chem. - Eur. J.* 2016, 22 (14), 4789–4793, DOI: 10.1002/chem.201504912
40. Li, Z.-L.; Wang, W.; Li, M.; Zhang, M.-J.; Tang, M.-J.; Su, Y.-Y.; Liu, Z.; Ju, X.-J.; Xie, R.; Chu, L.-Y. *Ind. Eng. Chem. Res.* 2018, 57 (13), 4562–4570, DOI: 10.1021/acs.iecr.7b04941
41. Zhang, Z.; Zhao, A.; Wang, F.; Ren, J.; Qu, X. *Chem. Commun.* 2016, 52 (32), 5550–5553, DOI: 10.1039/C6CC00910G
42. Mushtaq, F.; Asani, A.; Hoop, M.; Chen, X.-Z.; Ahmed, D.; Nelson, B. J.; Pané, S. *Adv. Funct. Mater.* 2016, 26 (38), 6995–7002, DOI: 10.1002/adfm.201602315
43. Singh, V. V.; Martin, A.; Kaufmann, K.; de Oliveira, S. D. S.; Wang, J. *Chem. Mater.* 2015, 27 (23), 8162–8169, DOI: 10.1021/acs.chemmater.5b03960
44. Wani, O. M.; Safdar, M.; Kinnunen, N.; Jänis, J. *Chem. - Eur. J.* 2016, 22 (4), 1244–1247, DOI: 10.1002/chem.201504474
45. He, X.; Bahk, Y. K.; Wang, J. *Chemosphere* 2017, 184, 601–608, DOI: 10.1016/j.chemosphere.2017.06.011
46. Mou, F.; Kong, L.; Chen, C.; Chen, Z.; Xu, L.; Guan, J. *Nanoscale* 2016, 8 (9), 4976–4983, DOI: 10.1039/C5NR06774J
47. Zhang, Q.; Dong, R.; Wu, Y.; Gao, W.; He, Z.; Ren, B. *ACS Appl. Mater. Interfaces* 2017, 9 (5), 4674–4683, DOI: 10.1021/acsami.6b12081
48. Mushtaq, F.; Guerrero, M.; Sakar, M. S.; Hoop, M.; Lindo, A. M.; Sort, J.; Chen, X.; Nelson, B. J.; Pellicer, E.; Pané, S. *J. Mater. Chem. A* 2015, 3 (47), 23670–23676, DOI: 10.1039/C5TA05825B
49. Orozco, J.; Mercante, L. A.; Pol, R.; Merkoçi, A. Graphene-based Janus micromotors for the dynamic removal of pollutants. *J. Mater. Chem. A* 2016, 4 (9), 3371–3378, DOI: 10.1039/C5TA09850E
50. Singh, V. V.; Jurado-Sánchez, B.; Sattayasamitsathit, S.; Orozco, J.; Li, J.; Galarnyk, M.; Fedorak, Y.; Wang, J. *Adv. Funct. Mater.* 2015, 25 (14), 2147–2155, DOI: 10.1002/adfm.201500033
51. Orozco, J.; Vilela, D.; Valdés-Ramírez, G.; Fedorak, Y.; Escarpa, A.; Vazquez-Duhalt, R.; Wang, J. *Chem. - Eur. J.* 2014, 20 (10), 2866–2871, DOI: 10.1002/chem.201304179

52. Zhao, G.; Pumera, M. *Lab Chip* 2014, 14 (15), 2818– 2823, DOI: 10.1039/C4LC00431K
53. Sattayasamitsathit, S.; Kaufmann, K.; Galarnyk, M.; Vazquez-Duhalt, R.; Wang, J. *RSC Adv.* 2014, 4 (52), 27565– 27570, DOI: 10.1039/C4RA04341C
54. Campuzano, S.; Orozco, J.; Kagan, D.; Guix, M.; Gao, W.; Sattayasamitsathit, S.; Claussen, J. C.; Merkoçi, A.; Wang, J. *Nano Lett.* 2012, 12 (1), 396– 401, DOI: 10.1021/nl203717q
55. Kiristi, M.; Singh, V. V.; Esteban-Fernández de Ávila, B.; Uygun, M.; Soto, F.; Aktaş Uygun, D.; Wang, J. *ACS Nano* 2015, 9 (9), 9252– 9259, DOI: 10.1021/acs.nano.5b04142
56. Delezuk, J. A. M.; Ramírez-Herrera, D. E.; Esteban-Fernández de Ávila, B.; Wang, J.; Li, J.; Wang, J.; Orozco, J.; Galarnyk, M.; Wang, J.; Wang, J. *Nanoscale* 2017, 9 (6), 2195– 2200, DOI: 10.1039/C6NR09799E
57. Vilela, D.; Stanton, M. M.; Parmar, J.; Sánchez, S. *ACS Appl. Mater. Interfaces* 2017, 9 (27), 22093– 22100, DOI: 10.1021/acsami.7b03006
58. Hoop, M.; Shen, Y.; Chen, X.-Z.; Mushtaq, F.; Iuliano, L. M.; Sakar, M. S.; Petruska, A.; Loessner, M. J.; Nelson, B. J.; Pané, S. *Adv. Funct. Mater.* 2016, 26 (7), 1063– 1069, DOI: 10.1002/adfm.201504463
59. Ge, Y.; Liu, M.; Liu, L.; Sun, Y.; Zhang, H.; Dong, B. *Nano-Micro Lett.* 2016, 8 (2), 157– 164, DOI: 10.1007/s40820-015-0071-3
60. Stanton, M. M.; Simmchen, J.; Ma, X.; Miguel-López, A.; Sánchez, S. *Adv. Mater. Interfaces* 2016, 3 (2), 1500505, DOI: 10.1002/admi.201500505
61. Simmchen, J.; Baeza, A.; Miguel-Lopez, A.; Stanton, M. M.; Vallet-Regi, M.; Ruiz-Molina, D.; Sánchez, S. *ChemNanoMat* 2017, 3 (1), 65– 71, DOI: 10.1002/cnma.201600300
62. Orozco, J.; Pan, G.; Sattayasamitsathit, S.; Galarnyk, M.; Wang, J. *Analyst* 2015, 140 (5), 1421– 1427, DOI: 10.1039/C4AN02169J
63. Kagan, D.; Calvo-Marzal, P.; Balasubramanian, S.; Sattayasamitsathit, S.; Manesh, K. M.; Flechsig, G.-U.; Wang, J. *J. Am. Chem. Soc.* 2009, 131 (34), 12082– 12083, DOI: 10.1021/ja905142q
64. Orozco, J.; García-Gradilla, V.; D'Agostino, M.; Gao, W.; Cortés, A.; Wang, J. *ACS Nano* 2013, 7 (1), 818– 824, DOI: 10.1021/nn305372n
65. Singh, V. V.; Kaufmann, K.; Esteban-Fernández de Ávila, B.; Uygun, M.; Wang, J. *Chem. Commun.* 2016, 52 (16), 3360– 3363, DOI: 10.1039/C5CC10670B
66. Moo, J. G. S.; Wang, H.; Zhao, G.; Pumera, M. *Chem. - Eur. J.* 2014, 20 (15), 4292– 4296, DOI: 10.1002/chem.201304804
67. Singh, V. V.; Kaufmann, K.; Orozco, J.; Li, J.; Galarnyk, M.; Arya, G.; Wang, J. *Chem. Commun.* 2015, 51 (56), 11190– 11193, DOI: 10.1039/C5CC04120A
68. Esteban-Fernández de Ávila, B.; Lopez-Ramirez, M. A.; Báez, D. F.; Jodra, A.; Singh, V. V.; Kaufmann, K.; Wang, J. *ACS Sens* 2016, 1 (3), 217– 221, DOI: 10.1021/acssensors.5b00300
69. Molinero-Fernández, Á.; Moreno-Guzmán, M.; López, M. Á.; Escarpa, A. *Anal. Chem.* 2017, 89 (20), 10850– 10857, DOI: 10.1021/acs.analchem.7b02440

70. Molinero-Fernández, Á.; Jodra, A.; Moreno-Guzmán, M.; López, M. Á.; Escarpa, A. *Chem. - Eur. J.* 2018, 24, 7172, DOI: 10.1002/chem.201706095
71. Jurado-Sánchez, B.; Pacheco, M.; Rojo, J.; Escarpa, A. *Angew. Chem., Int. Ed.* 2017, 56 (24), 6957– 6961, DOI: 10.1002/anie.201701396
72. Pacheco, M.; Jurado-Sánchez, B.; Escarpa, A. *Anal. Chem.* 2018, 90 (4), 2912– 2917, DOI: 10.1021/acs.analchem.7b05209
73. Jurado-Sánchez, B.; Escarpa, A.; Wang, J. *Chem. Commun.* 2015, 51 (74), 14088– 14091, DOI: 10.1039/C5CC04726A
74. Rojas, D.; Jurado-Sánchez, B.; Escarpa, A. *Anal. Chem.* 2016, 88 (7), 4153– 4160, DOI: 10.1021/acs.analchem.6b00574
75. Ma, X.; Hortelão, A. C.; Patiño, T.; Sánchez, S. *ACS Nano* 2016, 10 (10), 9111– 9122, DOI: 10.1021/acsnano.6b04108
76. Ma, X.; Wang, X.; Hahn, K.; Sánchez, S. *ACS Nano* 2016, 10 (3), 3597– 3605, DOI: 10.1021/acsnano.5b08067
77. Moo, J. G. S.; Wang, H.; Zhao, G.; Pumera, M. *Chem. - Eur. J.* 2014, 20 (15), 4292– 4296, DOI: 10.1002/chem.201304804
78. He, X.; Bahk, Y. K.; Wang, J. *Chemosphere* 2017, 184, 601– 608, DOI: 10.1016/j.chemosphere.2017.06.011
79. Simmchen, J.; Magdanz, V.; Sanchez, S.; Chokmaviroj, S.; Ruiz-Molina, D.; Baeza, A.; Schmidt, O. G. *RSC Adv.* 2014, 4 (39), 20334– 20340, DOI: 10.1039/C4RA02202E
80. Wang, H.; Zhao, G.; Pumera, M. *J. Phys. Chem. C* 2014, 118 (10), 5268– 5274, DOI: 10.1021/jp410003e
81. Villa, K.; Parmar, J.; Vilela, D.; Sánchez, S. *RSC Adv.* 2018, 8 (11), 5840– 5847, DOI: 10.1039/C7RA11705A